

Analysis of Connection Way of a Three-Dimensional Receiving Coil Onboard a Capsule Robot for Wireless Power Transmission

Jinyang Gao^{1, *}, Guozheng Yan², Yunbo Shi¹, Huiliang Cao¹,
Kun Huang¹, Hui Gao¹, and Jun Liu¹

Abstract—Wireless power transmission (WPT) based on near-field inductive coupling is a promising solution to power a tether-less capsule robot (CR) for medical application, and it is normally implemented with a one-dimensional transmitting coil for exciting an alternating magnetic field and an three-dimensional (3-D) receiving coil onboard the CR for induction. The connection way of the 3-D receiving coil has an influence on its output power supplied to the CR, but a method for quickly selecting series/parallel connection is not available yet. This paper is dedicated to developing such a method. Firstly, an analytical expression of the output power of the 3-D receiving coil when selecting series/parallel connection was derived, and its correctness was experimentally validated: the calculated output power using the analytical expression matched well with the measured one, having an average deviation of 1.42%/0.57% when selecting series/parallel connection. Then, a criterion for quickly selecting the connection way was deduced from the analytical expression, which indicates that the connection way is much related to the CR load: when the CR load is smaller than a critical load, parallel connection enables a larger output power average; otherwise, series connection does. A calculation method of the critical load is also given, which can be determined by available parameters relating to the transmitting coil and 3-D receiving coil. Thus, this paper provides a guidance for quickly selecting the connection way of the 3-D receiving coil.

1. INTRODUCTION

A capsule robot (CR) is a highly integrated micro-device that can be introduced from mouth/anus and can move actively in the intestine. It represents a promising medical technology for a minimally invasive diagnosis/treatment in the gastrointestinal (GI) tract [1–5]. Power supply is one of the bottlenecks limiting the CR application in clinical practice, because a power cable can cause a friction with the intestine which weakens the CR locomotion performance, and a button battery has limited capacity which is not sufficient to power the CR for long duration [6]. Wireless power transmission (WPT) based on near-field inductive coupling can supply hundreds of milliwatts to the CR timelessly and has been considered as one of the most promising solutions to the CR power supply issue [7–9].

WPT is normally implemented with a one-dimensional transmitting coil and a three-dimensional (3-D) receiving coil. The former excites an alternating magnetic field in a patient's abdominal area, and the latter is onboard the CR for induction. The induced electromotive force (EMF) of the 3-D receiving coil can be used to power the CR after being rectified and stabilized. A lot of studies involving design and optimization of the transmitting and receiving coils have been conducted in the literature, with an aim of maximizing power supplied to the CR under the precondition of ensuring human safety [10–14]. For example, the structure and number of turns of the transmitting coil have been optimized to

Received 29 October 2018, Accepted 3 January 2019, Scheduled 17 January 2019

* Corresponding author: Jinyang Gao (g.jy.1001@163.com).

¹ Science and Technology on Electronic Test and Measurement Laboratory, North University of China, Taiyuan 030051, China.

² Department of Instrument Science and Engineering, Shanghai Jiaotong University, Shanghai 200240, China.

improve the intensity and uniformity of the excited alternating magnetic field [10–12]; a ferrite core has been inserted within the receiving coil to enhance its coupling with the transmitting coil [13], and its geometrical shape has been designed to match the available space within the CR to improve space utilization [14]. However, a guidance for quickly selecting the connection way of the 3-D receiving coil, i.e., should the rectified EMFs of the three dimensional coils be superimposed in series/parallel, is not available yet. The selection is made based on experimental comparison currently, which has low efficiency and is tedious. This paper is dedicated to developing a method for quickly selecting the connection way of the 3-D receiving coil. With the basis of WPT theory and by analyzing the on-off characteristic and power loss of the rectifier, an analytical expression of the output power when selecting series/parallel connection is derived, and its correctness is verified with a cylinder-like 3-D receiving coil prototype and a specially designed WPT platform. Then a criterion for selecting a better connection way is deduced based on the analytical expression, and its effectiveness is also verified.

This paper is organized as follows. Section 2 presents the working principle of the WPT system for powering the CR. Section 3 derives the analytical expression of the output power of the 3-D receiving coil and the criterion for selecting the connection way. Section 4 designs experiment to validate the derived analytical expression and criterion, and Section 5 concludes.

2. WORKING PRINCIPLE OF WPT SYSTEM

Figure 1 shows the equivalent circuit of the WPT system based on near-field inductive coupling, which includes a primary side and a secondary side.

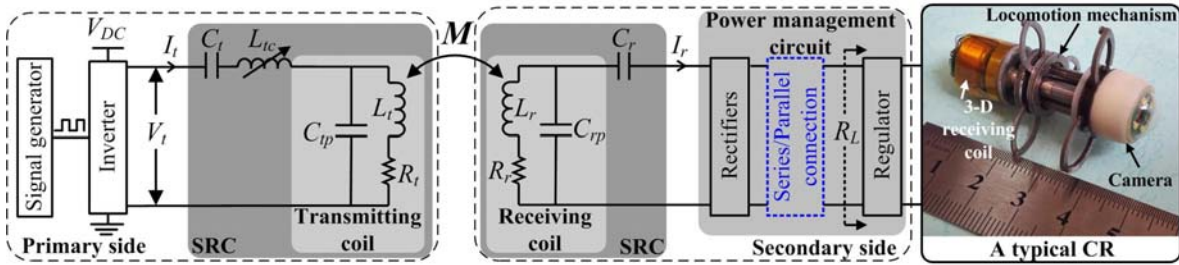


Figure 1. Equivalent circuit of the WPT system based on near-field inductive coupling.

The primary side consists of a signal generator for producing a square wave signal, a full-bridge inverter for converting a DC voltage V_{DC} to an AC pulse voltage V_t under the control of the square wave signal, and a serial resonant circuit (SRC) for exciting an alternating magnetic field when V_t is loaded on it. The SRC includes a vacuum capacitor C_t , an adjustable inductor L_{tc} , and a transmitting coil which is equivalent to a lumped-parameter circuit containing a self inductance L_t , an AC resistance R_t , and a parasitic capacitance C_{tp} ; here C_t and L_{tc} are used for making the transmitting coil resonate at a specific transmission frequency f .

The secondary side consists of an SRC for induction and a power management circuit for converting the induced EMF to a steady DC voltage to power the CR. The SRC at the secondary side includes a receiving coil (equivalent to a circuit containing a self inductance L_r , an AC resistance R_r , and a parasitic capacitance C_{rp}) and a tuning capacitor C_r to make the receiving coil resonate at the transmission frequency f . The power management circuit includes several rectifiers and a low-dropout regulator. The former converts the induced EMF to a pulsating DC voltage, and the latter regulates the pulsating DC voltage to be steady and in low noise. The series/parallel connection of the rectified EMFs of the three dimensional coils is implemented by connecting wires (referring to Fig. 4). For the convenience of analyzing the influence of the connection way on the output power, the low-dropout regulator and CR are equivalent to a load R_L in the analysis below.

When AC pulse voltage V_t is loaded on the SRC at the primary side, a sinusoidal driving current I_t ($= I_m \sin(2\pi ft)$ where I_m is the peak driving current) is generated in the transmitting coil because of the frequency-selection function of the SRC, and the alternating magnetic field is excited then. A

mutual inductance M between the transmitting coil and receiving coil makes the latter induce an EMF ε :

$$\varepsilon = M \frac{dI_t}{dt} \Rightarrow \varepsilon_{rms} = \sqrt{\frac{1}{T} \int_0^T \varepsilon^2 dt} = \sqrt{2} \pi f M I_m \quad (1)$$

where ε_{rms} is the root mean square of ε .

3. ANALYSIS ON SERIES/PARALLEL CONNECTION

3.1. Attitude Definition of 3-D Receiving Coil

Figure 2 shows a typical 3-D receiving coil, which is cylinder-like and is composed of a ferrite core, a rectangular coil a , a rectangular coil b , and a circular coil c . The ferrite core is cylinder-like but has some grooves on its lateral and end surfaces to supply winding space for coil a and coil b , and coil c is wound around its lateral surface. To define the attitude of the 3-D receiving coil, an attitude function is introduced:

$$\begin{aligned} g_a(\theta_1, \theta_2) &= \cos \theta_1 \cos \theta_2 \\ g_b(\theta_1, \theta_2) &= \sin \theta_1 \cos \theta_2 \\ g_c(\theta_1, \theta_2) &= \sin \theta_2 \end{aligned} \quad (2)$$

where $g_i (i = a, b, c)$ represents the attitude of coil i which ranges from 0 to 1, and θ_1 and θ_2 are the attitude angles pivoting axes OX and OY , respectively, as shown in Fig. 2. When $\theta_1 = 0^\circ$ and $\theta_2 = 0^\circ$, the normals of the planes enclosed by coils a , b , and c are along axes OZ , OY , and OX , respectively. When θ_1 and θ_2 range from 0° to 90° , the 3-D receiving coil suffers all possible attitudes because it is designed to be axisymmetric. Assuming that the alternating magnetic field is in OZ direction, the mutual inductance between the transmitting coil and coil i can be written as:

$$M_i = N_i M_0^i g_i \quad (i = a, b, c) \quad (3)$$

where N_i is the number of turns of coil i , and M_0^i is the single-turn mutual inductance when the enclosed plane of coil i is vertical to the alternating magnetic field direction. By substituting Eq. (3) into Eq. (1), the root-mean-square EMF of coil $i (i = a, b, c)$ can be rewritten as:

$$\varepsilon_{rms}^i = \sqrt{2} \pi f I_m N_i M_0^i g_i \quad (i = a, b, c) \quad (4)$$

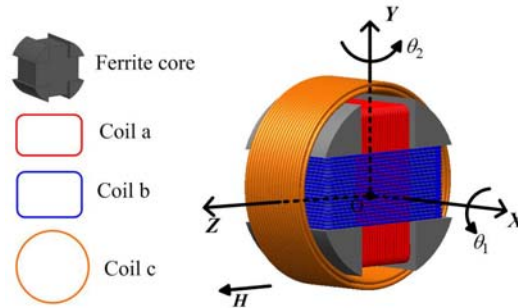


Figure 2. 3-D receiving coil and its attitude definition.

3.2. On-Off Characteristic and Power Loss of Full-Bridge Rectifier

Because coils a , b , and c can be respectively resonated by selecting proper tuning capacitors, the SRC at the secondary side in Fig. 1 can be equivalent to a power source having a root-mean-square EMF ε_{rms} in series with a equivalent series resistance (ESR) R_S which is related to L_r , R_r , C_{rp} and the transmission frequency f [15], as shown in Fig. 3. The following takes one-dimensional coil as an example, derives

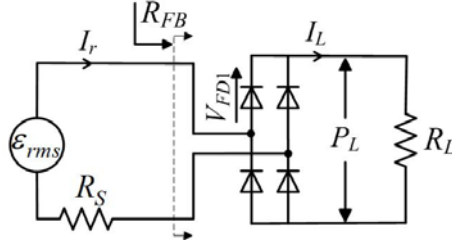


Figure 3. Simplified equivalent circuit of the secondary side.

the analytical expression of the output power P_L by analyzing the on-off characteristic and power loss of the full-bridge rectifier.

Denoting the input resistance of the full-bridge rectifier with R_{FB} , the input current of the full-bridge rectifier can be calculated as:

$$I_r = \sqrt{2}\varepsilon_{rms} \cos(2\pi ft) / (R_S + R_{FB}) \quad (5)$$

The electric charge flows through load R_L is equal to that flows into the full-bridge rectifier in a time period:

$$I_L T = \int_0^T |I_r| dt \quad (6)$$

where I_L is the average of the current flowing through R_L in a time period, and $T (= 1/f)$ is the time period. By substituting Eq. (5) into Eq. (6), the expression of I_L is obtained:

$$I_L = 2\sqrt{2}\varepsilon_{rms} / [\pi(R_S + R_{FB})] \quad (7)$$

The input-output power relationship of the full-bridge rectifier is:

$$P_{FB} = P_{FB}^{loss} + P_L \quad (8a)$$

$$P_{FB} = \frac{\varepsilon_{rms}^2}{(R_S + R_{FB})^2} R_{FB} \quad (8b)$$

$$P_{FB}^{loss} = \frac{2V_{FD1}}{T} \int_0^T |I_r| dt = \frac{4\sqrt{2}\varepsilon_{rms}V_{FD1}}{\pi(R_S + R_{FB})} \quad (8c)$$

$$P_L = I_L^2 R_L = 8\varepsilon_{rms}^2 R_L / [\pi(R_S + R_{FB})]^2 \quad (8d)$$

where P_{FB} , P_{FB}^{loss} , and P_L are the input power, power loss, and output power of the full-bridge rectifier, respectively. V_{FD1} is the forward voltage drop of the diode in the full-bridge rectifier. The coefficient “2” is multiplied when calculating P_{FB}^{loss} because there are always two diodes in a time period T . From Eq. (8), R_{FB} can be easily deduced as:

$$R_{FB} = \frac{8\sqrt{2}\varepsilon_{rms}R_L + 8\pi V_{FD1}R_S}{\sqrt{2}\pi^2\varepsilon_{rms} - 8\pi V_{FD1}} \quad (9)$$

By substituting R_{FB} in Eq. (8d) with Eq. (9), the analytical expression of the output power P_L is obtained:

$$P_L = \frac{4R_L(\sqrt{2}\pi\varepsilon_{rms} - 8V_{FD1})^2}{(\pi^2R_S + 8R_L)^2} \quad (10)$$

3.3. Output Power of 3-D Receiving Coil

Figures 4(a) and (b) show the equivalent circuits of the 3-D receiving coil when being connected in series and in parallel, respectively. When the rectified ε_{rms}^a , ε_{rms}^b , and ε_{rms}^c are connected in series, the total root-mean-square EMF of the 3-D receiving coil is $\sum \varepsilon_{rms}^i$ ($i = a, b, c$) and the total ESR is $\sum R_S^i$ ($i = a, b, c$), while when connected in parallel, only the coil having maximum output power is on

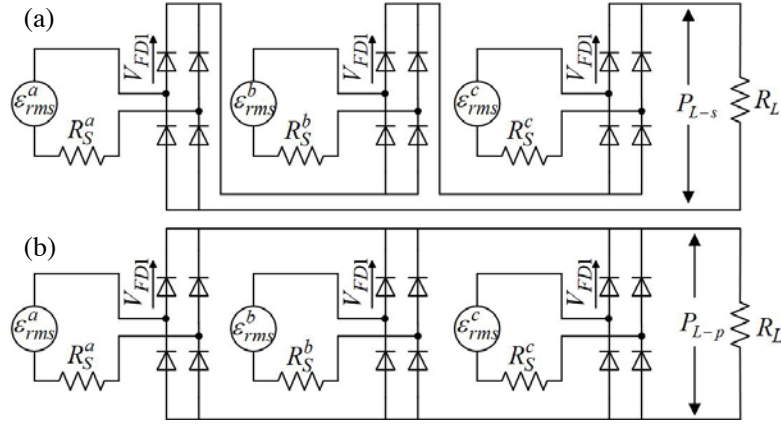


Figure 4. Equivalent circuits of the 3-D receiving coil when connected (a) in series and (b) in parallel.

because of diode-clamp function, and the total root-mean-square EMF and ESR of the 3-D receiving coil are equal to those of this coil, respectively. In addition, it can be found that there are six diodes always in the series case while only two in the parallel case; therefore, the rectification loss in the series case is three times larger than that in the parallel case when the same current flows through R_L .

Referring to Eq. (10), the analytical expressions of the output powers of the 3-D receiving when being connected in series and in parallel can be written as the follows, respectively:

$$P_{L-s} = \frac{4R_L(\sqrt{2}\pi \sum \varepsilon_{rms}^i - 24V_{FD1})^2}{(\pi^2 \sum R_S^i + 8R_L)^2} \quad i = a, b, c \quad (11a)$$

$$P_{L-p} = \max \left[\frac{4R_L(\sqrt{2}\pi \varepsilon_{rms}^i - 8V_{FD1})^2}{(\pi^2 R_S^i + 8R_L)^2} \right] \quad i = a, b, c \quad (11b)$$

3.4. Criterion for Selecting Series/Parallel Connection

It can be found from Eq. (4) and Eq. (11) that P_{L-s} and P_{L-p} are much related to the attitude of the 3-D receiving coil. Therefore, it is necessary to calculate the averages of P_{L-s} and P_{L-p} at all possible attitudes of the 3-D receiving coil when making a selection of series/parallel connection.

When designing a 3-D receiving coil, the electrical parameters of coils a , b , and c are expected to satisfy the following two equalities to minimize its output power fluctuation range [14]:

$$N_a M_0^a \approx N_b M_0^b \approx N_c M_0^c \quad (12a)$$

$$R_S^a \approx R_S^b \approx R_S^c \quad (12b)$$

Assuming that Eq. (12a) and Eq. (12b) both hold, Eq. (11) can be rewritten as:

$$P_{L-s} = \frac{4R_L[2\pi^2 f I_m N_i M_0^i (g_a + g_b + g_c) - 24V_{FD1}]^2}{(3\pi^2 R_S^i + 8R_L)^2} \quad i = a \text{ or } b \text{ or } c \quad (13a)$$

$$P_{L-p} = \frac{4R_L(2\pi^2 f I_m N_i M_0^i \max[g_a, g_b, g_c] - 8V_{FD1})^2}{(\pi^2 R_S^i + 8R_L)^2} \quad i = a \text{ or } b \text{ or } c \quad (13b)$$

The averages of $(g_a + g_b + g_c)^2$, $(g_a + g_b + g_c)$, $\max[g_a, g_b, g_c]^2$, and $\max[g_a, g_b, g_c]$ when θ_1 and θ_2 range from 0° to 90° can be easily computed as:

$$\begin{aligned} \overline{(g_a + g_b + g_c)^2} &= 2.1274 \\ \overline{g_a + g_b + g_c} &= 1.4467 \\ \overline{(\max[g_a, g_b, g_c])^2} &= 0.7470 \\ \overline{\max[g_a, g_b, g_c]} &= 0.8578 \end{aligned} \quad (14)$$

By substituting Eq. (14) into Eq. (13), the expressions of the averages of P_{L-s} and P_{L-p} at all possible attitudes are obtained:

$$\overline{P_{L-s}} = \frac{16R_L[2.1274\pi^4(fI_mN_iM_0^i)^2 - 34.7208\pi^2fI_mN_iM_0^iV_{FD1} + 144V_{FD1}^2]}{(3\pi^2R_S^i + 8R_L)^2} \quad i = a \text{ or } b \text{ or } c \quad (15a)$$

$$\overline{P_{L-p}} = \frac{16R_L[0.747\pi^4(fI_mN_iM_0^i)^2 - 6.8624\pi^2fI_mN_iM_0^iV_{FD1} + 16V_{FD1}^2]}{(\pi^2R_S^i + 8R_L)^2} \quad i = a \text{ or } b \text{ or } c \quad (15b)$$

Assuming $\overline{P_{L-s}} < \overline{P_{L-p}}$, the criterion for selecting series/parallel connection is deduced:

$$\begin{cases} R_L < R_{L-cri} = \frac{\sqrt{B^2 - 4AC} - B}{2A} \\ A = 88.3456\pi^4K^2 - 1782.9376\pi^2V_{FD1}K + 8192V_{FD1}^2 \\ B = -1.8176\pi^6R_S^iK^2 - 226.1376\pi^4V_{FD1}R_S^iK + 1536\pi^2V_{FD1}^2R_S^i \\ C = (-4.5956\pi^8K^2 + 27.0408\pi^6V_{FD1}K) \times (R_S^i)^2 \\ K = fI_mN_iM_0^i \end{cases} \quad i = a \text{ or } b \text{ or } c \quad (16)$$

The criterion indicates that the selection of the connection way is much related to the load R_L : when R_L is smaller than a critical load R_{L-cri} , parallel connection enables a larger output power average; otherwise, series connection does. The critical load R_{L-cri} can be calculated with parameters of R_S^i , N_i , M_0^i , V_{FD1} , f , and I_m , which are all available for given transmitting coil, 3-D receiving coil, full-bridge rectifier, and sinusoidal driving current flowing in the transmitting coil. Actually, the two equalities of Eq. (12) are not easy to be satisfied for a hand-making 3-D receiving coil; therefore when making a selection of the connection way using the criterion Eq. (16), R_S^i and $N_iM_0^i$ will be replaced with $(R_S^a + R_S^b + R_S^c)/3$ and $(N_aM_0^a + N_bM_0^b + N_cM_0^c)/3$, respectively.

4. EXPERIMENTS AND RESULTS

4.1. Experimental Setup

To verify the analysis above, the experimental setup shown in Fig. 5 is designed. A 3-D receiving coil prototype, whose structure is identical to that shown in Fig. 2, is installed at a two-axis turntable which can adjust its attitude by changing the attitude angles θ_1 and θ_2 (angle interval 5°). The two-axis

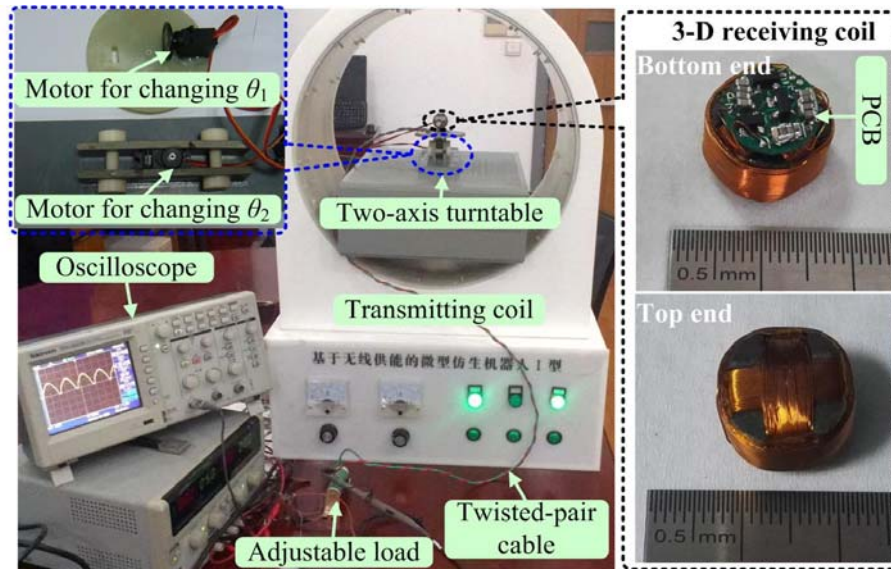


Figure 5. Experimental setup for measuring the output power of the 3-D receiving coil.

turntable is centered in the transmitting coil where the magnetic flux density has been verified minimum [8]. A PCB for welding the tuning capacitors and full-bridge rectifiers is fixed on the bottom end surface of the 3-D receiving coil, on which the rectification and series/parallel connection are both implemented. The full-bridge rectifier that employs here is a chip of BAS4002A (Infineon), and the forward voltage drop of its internal diode is $V_{FD1} = 0.27$ V. A twisted-pair cable, which can reduce conduction error by avoiding picking magnetic flux, is used to connect the PCB and an adjustable load (0–100 Ω), thus by measuring the terminal voltage of the adjustable load with an oscilloscope, the output power of the 3-D receiving coil can be obtained.

Table 1 lists the design parameters of the employed 3-D receiving coil prototype, which are selected to meet Eq. (12) as far as possible. However, small differences among the ESRs of coils a , b , c still exist because the proximity influence of the ferrite core on the ESR is intricate, and the manual winding process can introduce uncertain errors.

Table 1. Design parameters of the 3-D receiving coil.

Parameter	Coil a	Coil b	Coil c
Single-turn mutual inductance $M_0^i (\times 10^{-8} \text{ H})$	5.04	5.38	5.90
Number of turns N_i	96	90	82
ESR $R_S^i (\Omega)$	12.1	11.3	10.8
Ferrite core	Cylinder-like, R6K, $\Phi 12.5 \text{ mm} \times 8 \text{ mm}$		
Winding wire	Enameled copper wire with 0.15 mm diameter		
Overall size	$\Phi 13.8 \text{ mm} \times 8 \text{ mm}$		

The transmitting coil employed here is a pair of double-layer solenoids which is constructed by winding a litz wire (180 strands of AWG38 enameled copper wire) on a plastic hollow cylinder; it measures $\Phi 40 \text{ cm} \times 20 \text{ cm}$, and the number of turns of each layer is 25. With consideration of improving power transmission efficiency and ensuring human safety when being exposed to the alternating magnetic field, the transmission frequency and driving current peak of this transmitting coil have been optimized as $f = 218 \text{ KHz}$ and $I_m = 1.98 \text{ A}$, respectively [8].

4.2. Results and Discussion

Two tests were conducted using the experimental setup shown in Fig. 5: one for verifying the correctness of the analytical expression of the output power of the 3-D receiving coil, i.e., Eq. (11); the other for validating the effectiveness of the criterion for quickly selecting series/parallel connection, i.e., Eq. (16).

When verifying the correctness of Eq. (11), the adjustable load is set to $R_L = 21.78 \Omega$, which is a typical load value for a motor-driven capsule robot [16]. Fig. 6 shows the calculated P_{L-s} and P_{L-p} using Eq. (11), as well as the corresponding measurements, which can be concluded as follows.

Firstly, the calculated and measured P_{L-s} change identically with θ_1 and θ_2 . When $\theta_1 = 45^\circ$ and $\theta_2 = 35^\circ$, the calculated/measured P_{L-s} reaches a maximum of 1392/1374 mW. When $\theta_1 = 0^\circ$ and $\theta_2 = 0^\circ$, $\theta_1 = 90^\circ$ and $\theta_2 = 0^\circ$, and $\theta_2 = 90^\circ$, the calculated/measured P_{L-s} reaches a minimum of 398/341 mW, 399/366 mW, and 398/385 mW, respectively. The averages of the calculated and measured P_{L-s} when θ_1 and θ_2 range from 0° to 90° are respectively 918 mW and 905 mW, corresponding to a deviation of 1.42%.

Secondly, the calculated and measured P_{L-p} change identically with θ_1 and θ_2 , too. When $\theta_1 = 45^\circ$ and $\theta_2 = 35^\circ$, the calculated/measured P_{L-p} reaches a minimum of 521/559 mW. When $\theta_1 = 0^\circ$ and $\theta_2 = 0^\circ$, $\theta_1 = 90^\circ$ and $\theta_2 = 0^\circ$, and $\theta_2 = 90^\circ$, the calculated/measured P_{L-p} reaches a maximum of 1542/1540 mW, 1576/1604 mW, 1722/1715 mW, respectively. The averages of the calculated and measured P_{L-p} when θ_1 and θ_2 range from 0° to 90° are respectively 1234 mW and 1227 mW, corresponding to a deviation of 0.57%. The average of P_{L-p} is about 300 mW larger than that of P_{L-s} ; therefore, parallel connection should be selected when $R_L = 21.78 \Omega$.

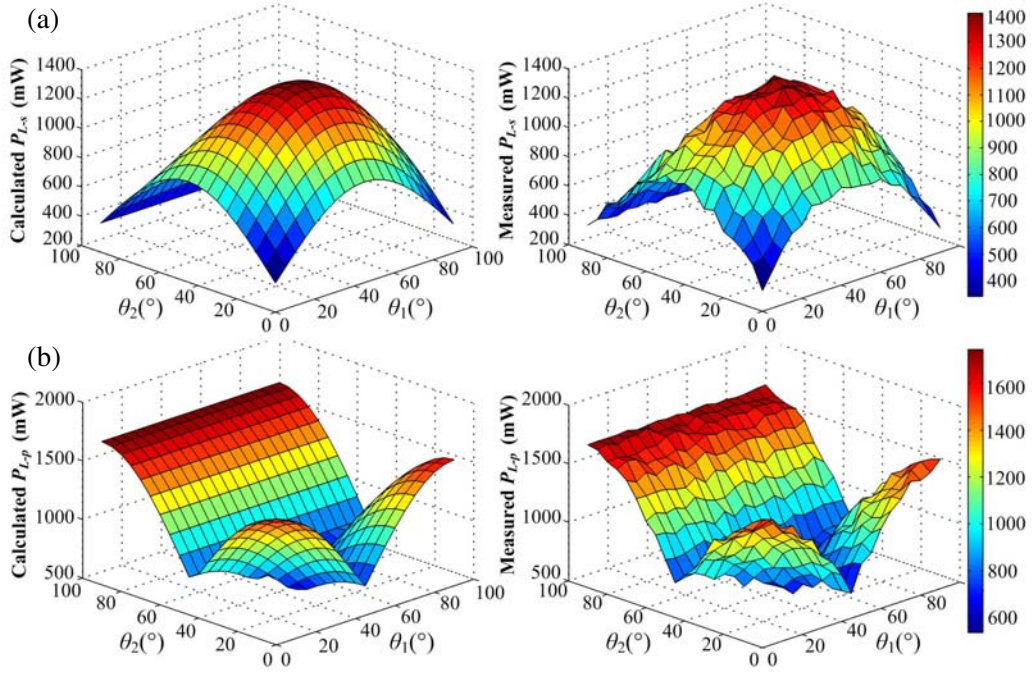


Figure 6. Output power of the 3-D receiving coil (a) P_{L-s} and (b) P_{L-p} when the attitude angles θ_1 and θ_2 range from 0° to 90° .

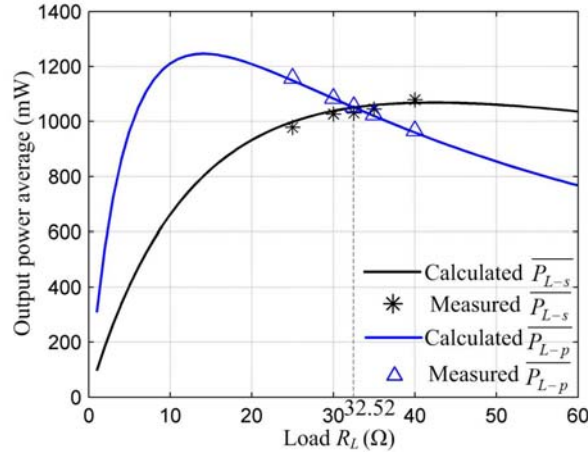


Figure 7. Changing of the output power average of the 3-D receiving coil with the load.

The above results show that the calculated P_{L-s} and P_{L-p} match well with the measured ones, thus confirming the correctness of Eq. (11). Note that the deviation in the parallel case is much smaller than that in the series case, which may be related to the number of error sources in the parallel case where one-dimensional coil, and two diodes are always on. The number of error sources in the parallel case is lower than that in the series case where three-dimensional coils, and six diodes are always on.

When validating the effectiveness of the criterion for selecting series/parallel connection, the critical load is calculated at first by substituting $R_S^i = (R_S^a + R_S^b + R_S^c)/3 = 11.4\Omega$, $N_i M_0^i = N_a M_0^a + N_b M_0^b + N_c M_0^c/3 = 483.95 \times 10^{-8} \text{ H}$, $V_{FD1} = 0.27 \text{ V}$, $f = 218 \text{ KHz}$, and $I_m = 1.98 \text{ A}$ into Eq. (16), which is $R_{L-cri} = 32.52\Omega$. Then the adjustable load is set to $R_L = 25\Omega$, 30Ω , 32.52Ω , 35Ω , and 40Ω in sequence, and the corresponding $\overline{P_{L-s}}$ and $\overline{P_{L-p}}$ are measured by firstly measuring P_{L-s} and P_{L-p} when θ_1 and θ_2 range from 0° to 90° then averaging the measurements. Fig. 7 shows the

measured $\overline{P_{L-s}}$ and $\overline{P_{L-p}}$, as well as the $\overline{P_{L-s}}$ and $\overline{P_{L-p}}$ curves calculated with Eq. (15). It can be found that:

Firstly, the calculated $\overline{P_{L-s}}$ and $\overline{P_{L-p}}$ both firstly increase and then decrease with the load R_L , and they reach maxima when R_L are respectively about 42Ω and 14Ω because of load matching, but the matched load resistances are slightly larger than $R_S^a + R_S^b + R_S^c$ and $(R_S^a + R_S^b + R_S^c)/3$, which can be considered as the equivalent internal resistances of the 3-D receiving coil when selecting series and parallel connections, respectively.

Secondly, the measured $\overline{P_{L-s}}$ and $\overline{P_{L-p}}$ basically match with the calculated curves. When $R_L = R_{L-cri} = 32.52\Omega$, the difference between the measured $\overline{P_{L-s}}$ and $\overline{P_{L-p}}$ is only 20 mW. When $R_L > R_{L-cri}$ and $R_L < R_{L-cri}$, the measured $\overline{P_{L-s}}$ is obviously larger and smaller than $\overline{P_{L-p}}$, respectively. Thus manifesting the criterion Eq. (16) is effective in guiding the selection of series/parallel connection. A capsule robot that can move actively normally has a load less than 30Ω and a passive capsule endoscopy larger than 60Ω ; therefore, parallel and series connections should be respectively selected when they are powered by the 3-D receiving coil.

5. CONCLUSIONS

In this paper, an analytical expression of the output power of the 3-D receiving coil when selecting series/parallel connection has been derived as Eq. (11), and based on which, a criterion for quickly selecting the connection way has been deduced as Eq. (14). The criterion indicates that the connection way is much related to the relative magnitude of load R_L and critical load R_{L-cri} which can be calculated with available parameters of R_S^i , N_i , M_0^i , V_{FD1} , f , and I_m : when $R_L < R_{L-cri}$, parallel connection enables a larger output power average; otherwise, series connection does. The correctness of the analytical expression and the effectiveness of the criterion have been verified with a cylinder-like 3-D receiving coil prototype and a specially designed WPT platform. The experimental results show that the measured output power matches well with those calculated by the analytical expression, and the deviation is only 1.42%/0.57% when selecting series/parallel connection; in addition, the changing of the measured output power average with the load R_L agrees well with that indicated by the criterion, manifesting that the criterion can provide a effective guidance for quickly selecting series/parallel connection of the 3-D receiving coil.

ACKNOWLEDGMENT

This research was partially supported by the National Natural Science Foundation of China (Grant No. 61803347, No. 61673271, No. 81601631), by Shanxi Province Science Foundation for Youths (Grant No. 201801D221201), by Youth Academic Leader Support Project of North University of China (Grant No. QX201808), by the Science and Technology Commission of Shanghai Municipality (Grant No. 15441903100), and by the Science and Technology on Electronic Test and Measurement Laboratory, North University of China (Grant No. WD614200104011804).

REFERENCES

1. Guo, S., Q. Yang, L. Bai, and Y. Zhao, "Development of multiple capsule robots in pipe," *Micromachines*, Vol. 9, No. 6, 259–274, 2018.
2. Park, H., D. Kim, and B. Kim, "A robotic colonoscope with long stroke and reliable leg clamping," *International Journal of Precision Engineering and Manufacturing*, Vol. 13, No. 8, 1461–1466, 2012.
3. Valdastrì, P., R. J. Webster, C. Quaglia, A. Menciasì, and P. Dario, "A new mechanism for mesoscale legged locomotion in compliant tubular environments," *IEEE Transactions on Robotics*, Vol. 25, No. 5, 1047–1057, 2009.
4. Gao, J., G. Yan, S. He, F. Xu, Z. Wang, "Design, analysis, and testing of a motor-driven capsule robot based on a sliding clasper," *Robotica*, Vol. 35, 521–536, 2017.

5. Kim, H. M., S. Yang, J. Kim, S. Park, J. H. Cho, J. Y. Park, T. S. Kim, E. Yoon, S. Y. Song, and S. Bang, "Active locomotion of a paddling-based capsule endoscope in an in vitro and in vivo experiment (with videos)," *Gastrointestinal Endoscopy*, Vol. 72, No. 2, 381–387, 2010.
6. Ciuti, G., A. Menciassi, and P. Dario, "Capsule endoscopy: From current achievements to open challenges," *IEEE Reviews in Biomedical Engineering*, Vol. 4, 59–72, 2012.
7. Carta, R., G. Tortora, J. Thoné, B. Lenaerts, P. Valdastri, A. Menciassi, P. Dario, and R. Puers, "Wireless powering for a self-propelled and steerable endoscopic capsule for stomach inspection," *Biosensors and Bioelectronics*, Vol. 25, No. 5, 845–851, 2010.
8. Jia, Z., G. Yan, Z. Wang, and H. Liu, "Efficiency optimization of wireless power transmission systems for active capsule endoscopes," *Physiological Measurement*, Vol. 32, No. 10, 1561–1573, 2011.
9. Basar, M. R., M. Y. Ahmad, J. Cho, and F. Ibrahim, "Application of wireless power transmission systems in wireless capsule endoscopy: An overview," *Sensors*, Vol. 14, No. 6, 10929–10951, 2014.
10. Ke, Q., W. Luo, G. Yan, and K. Yang, "Analytical model and optimized design of power transmitting coil for inductive coupled endoscope robot," *IEEE Transactions on Biomedical Engineering*, Vol. 63, No. 4, 694–706, 2016.
11. Basar, M. R., M. Y. Ahmad, J. Cho, and F. Ibrahim, "Stable and high-efficiency wireless power transfer system for robotic capsule using a modified helmholtz coil," *IEEE Transactions on Industrial Electronics*, Vol. 64, No. 2, 1113–1122, 2017.
12. Basar, M. R., M. Y. Ahmad, J. Cho, and F. Ibrahim, "An improved wearable resonant wireless power transfer system for biomedical capsule endoscope," *IEEE Transactions on Industrial Electronics*, Vol. 65, No. 10, 7772–7781, 2018.
13. Carta, R., J. Thoné, and R. Puers, "A wireless power supply system for robotic capsular endoscopes," *Sensors and Actuators A: Physical*, Vol. 162, No. 2, 177–183, 2010.
14. Gao, J., G. Yan, Z. Wang, S. He, F. Xu, P. Jiang, and D. Liu, "Design and testing of a motor-based capsule robot powered by wireless power transmission," *IEEE/ASME Transactions on Mechatronics*, Vol. 21, No. 2, 683–693, 2016.
15. Luo, W., Q. Ke, G. Yan, and K. Yang, "Analytical computation of AC resistance of single-layer air-core Helmholtz coils," *Progress in Electromagnetics Research C*, Vol. 51, 111–119, 2014.
16. Gao, J. and G. Yan, "A novel power management circuit using a super-capacitor array for wireless powered capsule robot," *IEEE/ASME Transactions on Mechatronics*, Vol. 22, No. 3, 1444–1455, 2017.